The rate of methane formation seemed to be somewhat stronger inhibited by CO than the rate of CO consumption, but the effect was difficult to quantify by adjusting the value of K_{CO}. Using a slightly modified version of equation 5–3 for the rate of methane formation seemed to cope with the problem. The rate expression for methane formation is shown i equation 5–4. The value of K_{CO} is the same in expression 5–3 and 5–4.

5.3.3. Rate expressions and parameter estimation

The rate expressions used in the kinetic model are shown in equations 5–3 and 5–4, and the complete set of equations is presented in Appendix III.

$$-r_{v,CO} = \frac{(1 - \beta_{CO} t)\, A_{CO}\, e^{-\frac{E_{CO}}{RT}} P_{CO}\, P_{H_2}}{(1 + K_{CO}\, P_{CO})^2} \qquad (5\text{–}3)$$

$$r_{v,CH_4} = \frac{(1 - \beta_{CH_4} t)\, A_{CH_4}\, e^{-\frac{E_{CH_4}}{RT}} P_{CO}^{1/2}\, P_{H_2}}{(1 + K_{CO}\, P_{CO})^2} \qquad (5\text{–}4)$$

The observed decline in catalyst activity was modeled using a constant rate of deactivation. The deactivation rate β was assumed independent of time and reactor position, but different for CO and CH_4. The parameters estimated from the experimental data were the modified preexponential factor A'_i, and deactivation rate β_i, in the rate expressions for CO and CH_4. The modified preexponential factor is defined in Appendix III.

The results are shown in Table 5–2 for the two selected sets of activation energies. Model input for the three runs are given in Table 4–2. The parameters were obtained by solving the steady state mass balance equations at the time of each concentration measurement, and comparing simulated and measured concentrations of CO and CH_4 using a least square criterion. The time at the first measurement in each run was arbitrarily set to zero. Initial catalyst activity is thus defined as the activity when the first gas phase analysis is taken.

Comparison of simulated and measured concentrations is shown in Figures 5–6 to 5–9 for the two sets of activation energies. Generally the fit is good and there is virtually no effect of the values of the activation energies on the goodness of fit.

Table 5–2. Estimated kinetic parameters.

K_{CO}	17.0					
E_{CO}	110 000			80 000		
E_{CH_4}	140 000			110 000		
Run no.	1	2	3	1	2	3
A'_{CO}	3.63×10^{-1}	5.18×10^{-1}	1.73×10^{-1}	4.06×10^{-1}	5.41×10^{-1}	1.85×10^{-1}
A'_{CH_4}	1.43×10^{-2}	1.98×10^{-2}	7.07×10^{-3}	1.69×10^{-2}	2.07×10^{-2}	7.50×10^{-3}
β_{CO}	4.26×10^{-3}	9.94×10^{-3}	1.86×10^{-2}	6.65×10^{-3}	9.85×10^{-3}	1.93×10^{-2}
β_{CH_4}	9.70×10^{-3}	2.01×10^{-2}	7.63×10^{-3}	1.58×10^{-2}	2.02×10^{-2}	7.66×10^{-3}

An irregularity is denoted on the simulation curves for run 1 at z = 0.75 m, especially for the methane concentration. This irregularity seems to be more pronounced for the higher activation energies. It turned out that the measured temperatures at this point were slightly lower than the temperatures at the next point which explains this irregulariy in the simulations. But the reason for this observation is not understood from the fact that the catalyst activity decreased with increasing time, causing a consecutive decrease in temperature.

Although the fit is good, the parameters in Table 5–2 should not be given a wider interpretation. The range of experimental conditions is narrow and there are several possibilities of model errors. Simplifications with possibly unknown effects have also been done: The activation energies and K_{CO} are not precisely known and may be dependent on time and reactor position. The rate of deactivation is most certainly a function of time and reactor position, and the parameter β may be regarded as a correction factor both for time and reactor position dependent variations in catalyst activity. The data of Table 5–2, however, shows that the catalyst activity in run 3 was lower than that of the two previous runs. That was expected due to the thermal runaway which occured during start up of run 3.

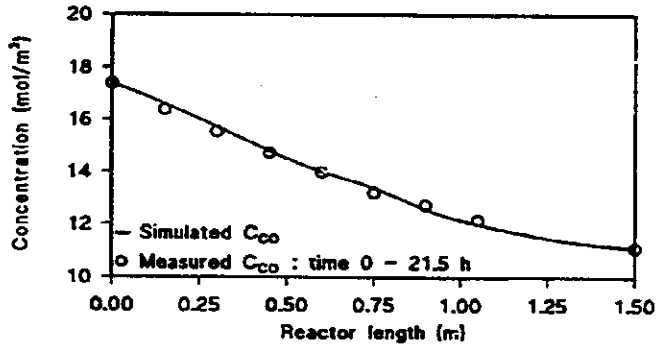

Run 1

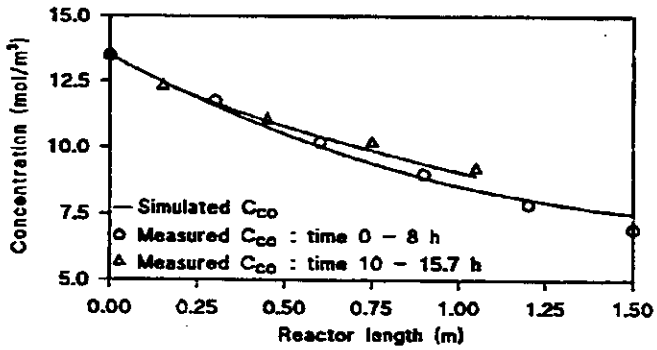

Run 2

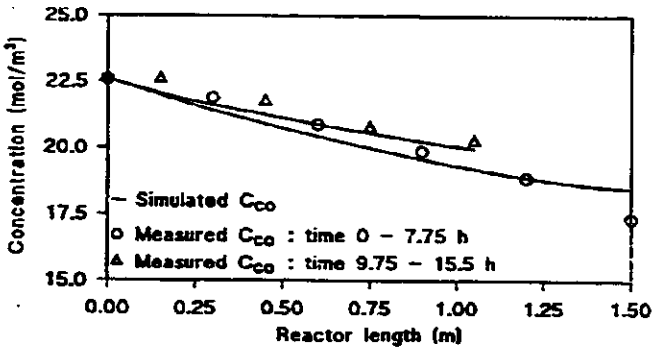

Run 3

Figure 5–6. Comparison of simulated and measured concentrations for kinetic parameters in table 5–2. E_{CO} = 110 kJ/mol, E_{CH_4} = 140 kJ/mol.

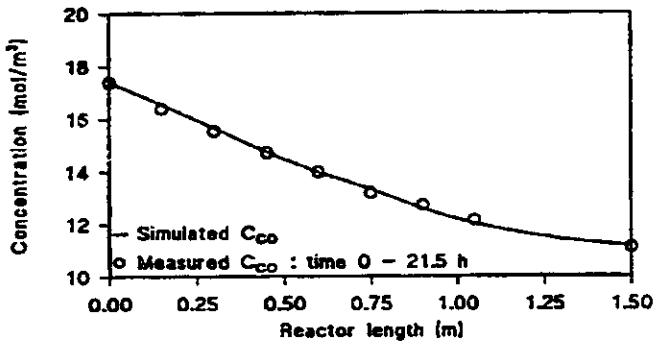

Run 1

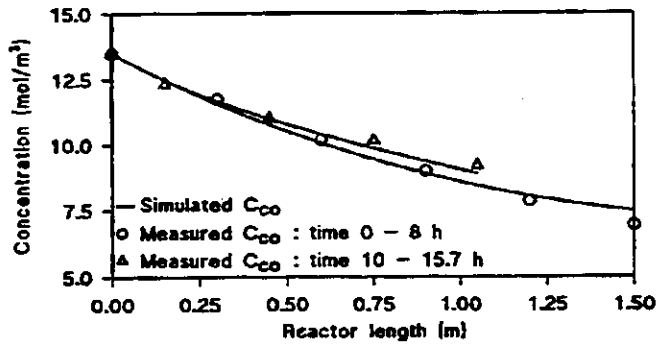

Run 2

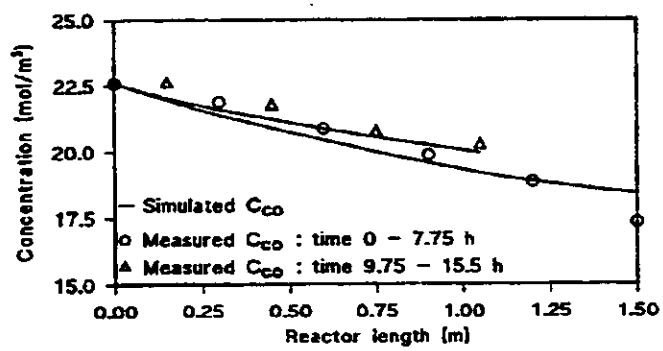

Run 3

Figure 5–7. Comparison of simulated and measured concentrations for kinetic parameters in table 5–2. E_{CO} = 80 kJ/mol, E_{CH_4} = 110 kJ/mol.

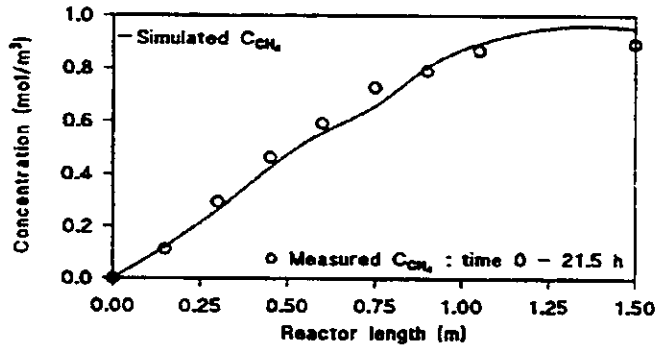

Run 1

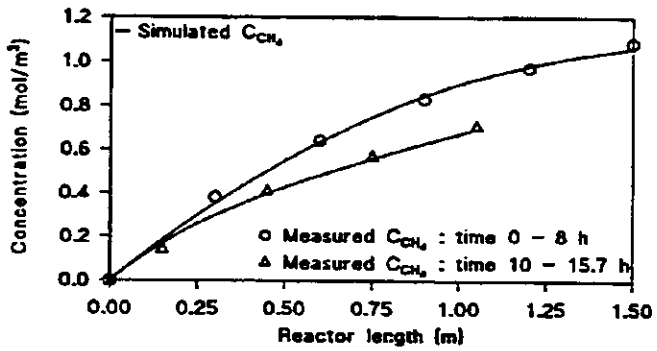

Run 2

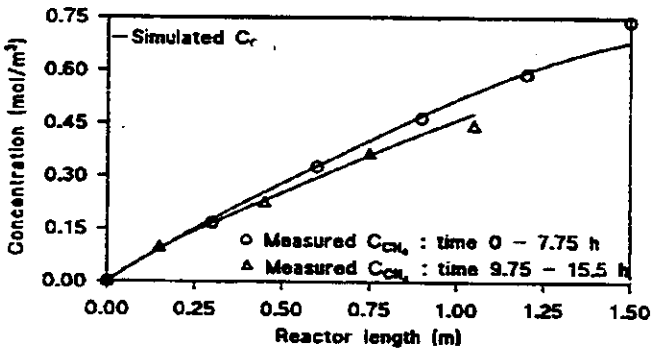

Run 3

Figure 5-8. Comparison of simulated and measured concentrations for kinetic parameters in table 5-2. E_{CO} = 110 kJ/mol, E_{CH_4} = 140 kJ/mol.

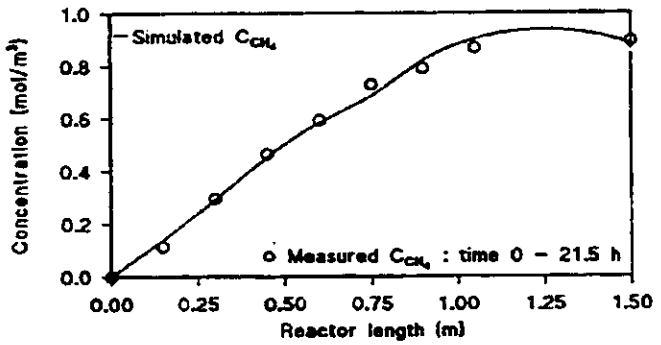

Run 1

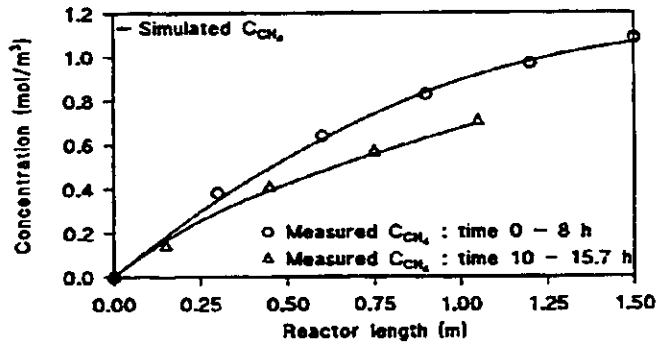

Run 2

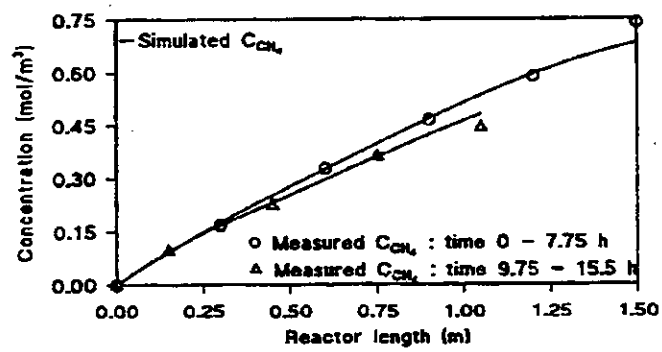

Run 3

Figure 5–9. Comparison of simulated and measured concentrations for kinetic parameters in table 5–2. E_{CO} = 80 kJ/mol, E_{CH_4} = 110 kJ/mol.

5.3.4. Effect of internal pellet diffusional resistance

It was speculated in the previous discussions that the long term decrease in catalyst activity was due to an increased fraction of the pores being filled up with liquid products, causing increased reactant diffusional resistance with increasing time. To see if this effect could explain the observed activity decline, some simulations were performed using the heterogeneous model.

Two assumptions were made about the internal pellet diffusional resistance. First it was assumed that only minor amounts of liquid was present in the catalyst pores, as is the case during the first period after start-up of a run. In this case only gas diffusional resistance need to be considered. Secondly it was assumed that the pores were completely filled with liquid, as is the case after long times on stream. The results were compared with calculations from the homogeneous model. The kinetic expressions 5–3 and 5–4 at initial activity (t=0) were used as the model for the intrinsic kinetics. The parameters were taken from Table 5–2 using the set of higher activation energies.

Due to the coupling between conversion and temperature, both heat and mass transfer had to be taken into account in the models. The traditional dispersion model with constant radial void fraction and velocity, evaluated in chapter 5.4, was used. Mass transfer resistance between solid and fluid phases was neglected, but heat transfer resistance was taken into account. The heat transfer coefficient between solid and fluid phases was calculated from equation 2–27 and the heat transfer resistance at the wall was calculated from equation 2–26. The fluid phase dispersion coefficients and other necessary data are given in chapter 4. The value of the effective radial conductivity was obtained from the estimations described in chapter 5.4.

The values of the gas phase effective pellet diffusivities were obtained from the molecular diffusivities given in Table 4–3 and the expression for Knudsen diffusivity given by Satterfield (Satterfield, 1970). Combining molecular and Knudsen diffusivities (Satterfield, 1970), correcting for pellet porosity and tortuosity which was taken to be 3, a value of $3 \cdot 10^{-7}$ m^2/s was obtained for CO and $1 \cdot 10^{-6}$ m^2/s for H_2.

The liquid phase effective pellet diffusivity of H_2 was estimated by Post et al. (Post et al., 1989) to be in the range, $0.9 \cdot 10^{-9} - 1.8 \cdot 10^{-9}$ m^2/s, based on gas phase concentrations, and the ratio between H_2 and CO effective diffusivities is about 2 (Iglesia et al., 1993). Due to numerical problems in solving the pellet equations with such low diffusivities, the values used in the simulations were somewhat higher than the values estimated by Post et al., $2 \cdot 10^{-9}$ m^2/s was used for CO and $4 \cdot 10^{-9}$ m^2/s for H_2. The result shown in Figure 5–10 for the conversion of CO was obtained using the conditions given in Table 4–2 for run no. 2.

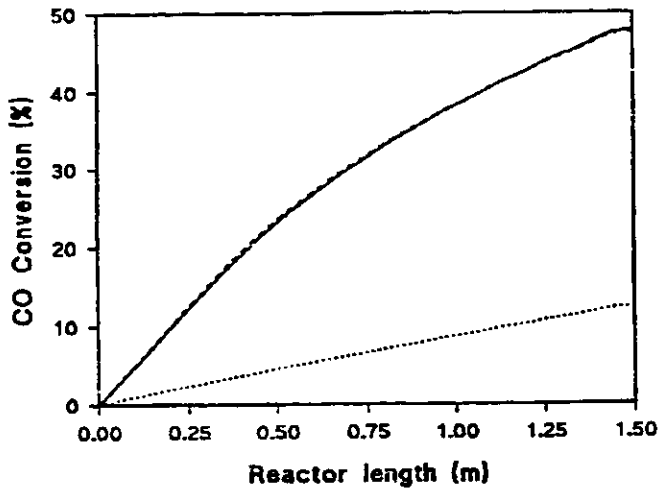

Figure 5–10. Effect of intraparticle diffusional resistance on CO conversion profile.

——, homogeneous model

——, gas phase resistance

------, liquid phase resistance

Although the values used for the liquid phase diffusivities were more than twice the values reported in the literature, it is shown in Figure 5–10 that the CO conversion is severely reduced by liquid phase diffusional resistance. The long term catalyst activity decline observed in the experiments is most likely due to increased diffusional resistance caused by accumulation of liquid products in the catalyst pores. Gas phase diffusional resistance seems not to have any significance at the experimental conditions employed in this study.

5.4. HEAT TRANSFER

5.4.1. Introduction

This chapter is concerned with the evaluation of the heat transfer characteristics of the pilot reactor based on the different approaches on heat transfer in packed beds which are reviewed in chapter 2.2.4 and further revealed in the following chapters.

In traditional dispersion models void fraction and velocity are assumed constant across the bed, and radial heat transfer is controlled by the effective conductivity of the bed and the heat transfer coefficient at the wall. However, heat transfer parameters estimated from experimental measurements using this approach show a great scatter between different published data and correlations (Tsotsas and Schlünder, 1990), especially at Reynolds numbers less than about 1000. The problem is that most fixed bed catalytic reactors fall into this range. In addition, substantial differences have been found between radial conductivity measured under reactive and non–reactive conditions.

Due to these problems, another concept based on locally varying radial dispersion coefficients due to the near–wall porosity and velocity changes has received attention in the recent time. This approach is the basis of the wall heat conduction model of Vortmeyer and Haidegger (Vortmeyer and Haidegger, 1991) described in chapter 2.2.7.

In the part of the work described in this chapter a comparison has been made between the traditional wall heat transfer model and the wall heat conduction model based on the experimental results obtained from the pilot reactor study. Both model types were adapted to give an optimal fit to experimental concentration and temperature profiles by estimation of parameters controlling radial heat transfer. These were parameters commonly encountered in correlations, and the values obtained were compared with values from the literature. These parameters and correlations are given in the next chapter. The adaption was obtained by fitting the model output to the experimental data of all the runs simultaneously, using a least square criterion.

5.4.2. Parameters and correlations

The heat transfer parameter estimated from the experimental data was the radial fluid–mechanical Peclet number for heat, Pe^{4}_{hr}, for the wall heat transfer model. This parameter is related to the effective radial Peclet number for heat through equation 5–5. The heat transfer coefficient at the wall was estimated from the correlation of Dixon and Cresswell (Dixon and Cresswell, 1979) shown in equation 2–26. The value used for this parameter showed up to be of less importance as the model solution was rather insensitive to variations in the value. This is an observation also denoted by others, e.g. (Vortmeyer and Haidegger, 1991).

$$\frac{1}{Pe_{hr}} = \frac{\lambda^{0}_{e}/\lambda_{g}}{Pe^{0}_{h}} + \frac{1}{Pe^{4}_{hr}} \qquad (5\text{–}5)$$

In the wall heat conduction model the effective radial conductivity is dependent on radial position. It is assumed that $\lambda_r(r)$ follows the relation given in equation 2–33. This relation is also shown in equation 5–6 with a slightly different notation.

$$\frac{\lambda_r(r)}{\lambda_g} = \frac{\lambda^{0}_{e}(r)}{\lambda_g} + CRe_p Pr \frac{v(r)}{v_0} f(1-r') \qquad (5\text{–}6)$$

The constant C in equation 5–6 was estimated from the experimental data with two different assumptions regarding the wall function f(1–r'). First it was assumed that the reactor wall affected the thermal conductivity in the near wall region in addition to the effect induced by the velocity profile in this region. This additional dependency was assumed to follow the relationship shown in equation 5–7.

$$f(1-r') = \begin{cases} \dfrac{R'}{l_w}(1-r') & \text{for } 0 \le (1-r') \le \dfrac{l_w}{R'} \\ 1 & \text{for } (1-r') > \dfrac{l_w}{R'} \end{cases} \qquad (5\text{–}7)$$

The wall function increases linearly from 0 at the wall to 1 at a distance of l_w particle diameters from the wall. In the interior of the bed the wall function has no effect. The distance l_w was chosen to be 2.5 particle diameters (Cheng and Vortmeyer, 1988) and 1 particle diameter (Schlünder, 1966; Hunt and Tien, 1990).

Secondly it was assumed that there was no effect in addition to the effect of the velocity profile in the near wall region. This gives the wall function:

$$f(1-r') = 1 \qquad \text{for all } r' \tag{5-8}$$

The relation of Vortmeyer and Schuster (Vortmeyer and Schuster, 1983) shown in equation 2-28 is used to approximate the radial void fraction profile. Because the parameter ε_w was unknown, the expression is regrouped as shown in equation 5-9. Relations for calculation of the constants C_1 and C_2 are given in Appendix IV.

$$\varepsilon(r) = C_1\left(1 + C_2 e^{\frac{2}{d_p}r}\right) \tag{5-9}$$

The velocity profiles were estimated from the analytical expression of Vortmeyer and Schuster (Vortmeyer and Schuster, 1983) shown in Appendix IV. This expression is based on solutions of the momentum equation 2-29 for the void fraction profile of equation 2-28.

The reactor model equations and all necessary parameter values and correlations are given in chapter 4, and the kinetic parameters are given in Table 5-2.

5.4.3. Results

A comparison between experimental and simulated reactor profiles for the optimal values of the parameters is shown in Figures 5-11 to 5-13. These are the temperature profiles and the concentration profiles of CO and CH_4. The model solutions are shown for the heat transfer model and for the heat conduction model with and without an additional wall function. Estimation of heat transfer parameters was performed for the two sets of activation energies used in the kinetic study.

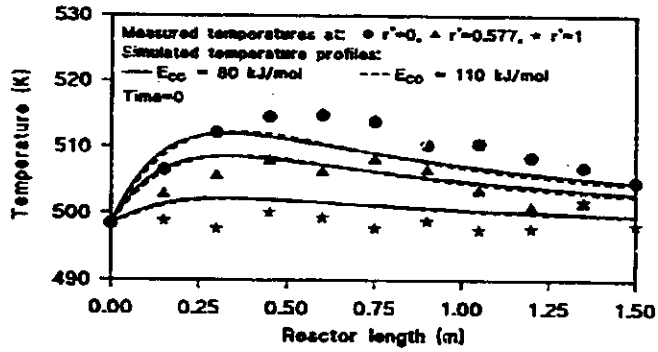

Wall heat transfer model.

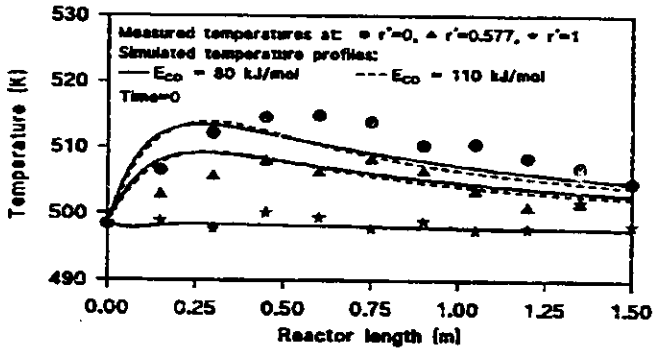

Wall heat conduction model. Wall function: Equation 5–12 $L_w = 1.0$

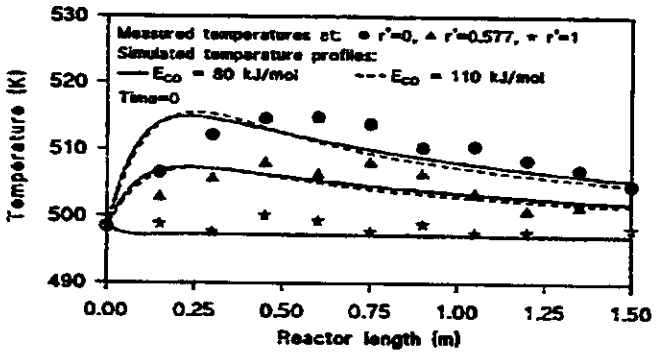

Wall heat conduction model. Wall function: Equation 5–13

Figure 5–11a. Comparison of simulated and measured temperature profiles. Run no 1.

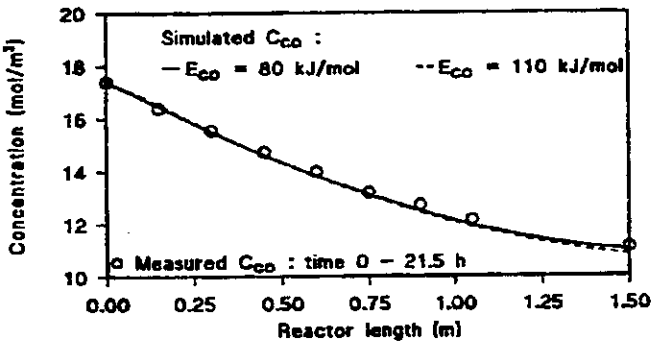

Wall heat transfer model.

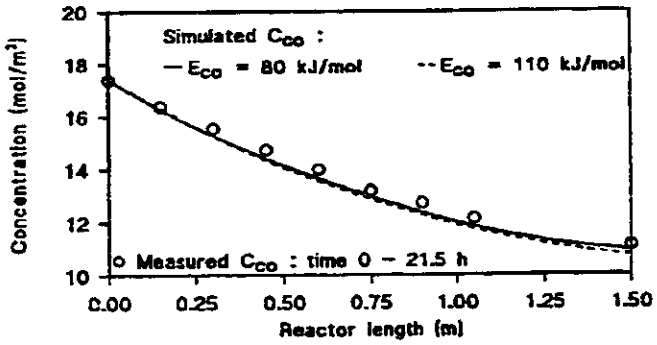

Wall heat conduction model. Wall function: Equation 5–12 L_w = 1.0

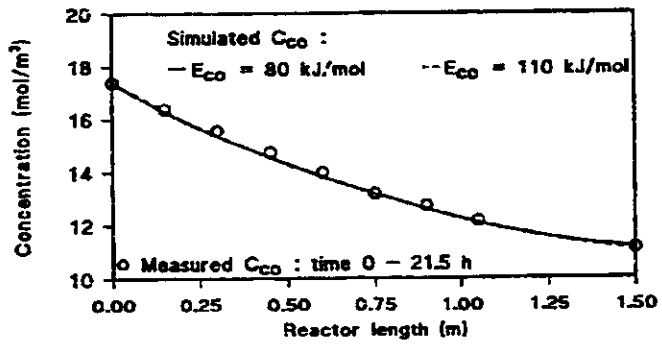

Wall heat conduction model. Wall function: Equation 5–13

Figure 5–11b. Comparison of simulated and measured CO profiles. Run no 1.

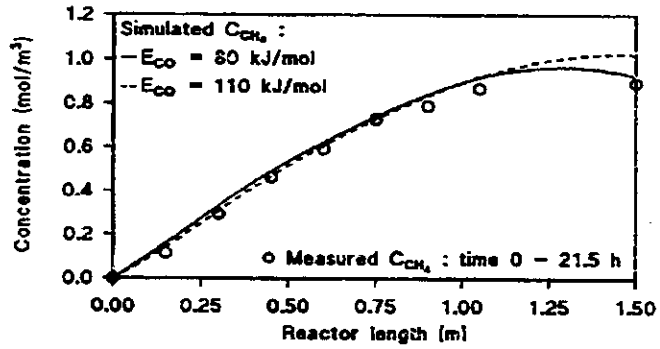

Wall heat transfer model.

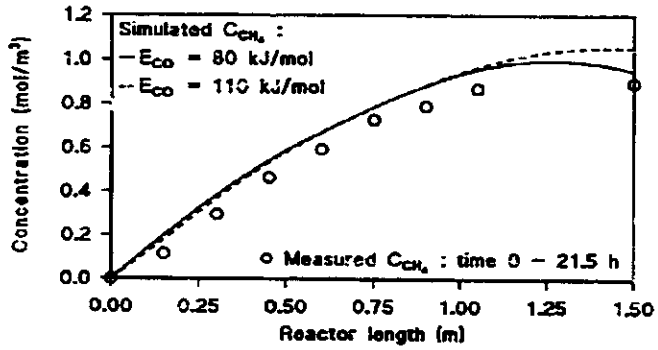

Wall heat conduction model. Wall function: Equation 5–12 L_w = 1.0

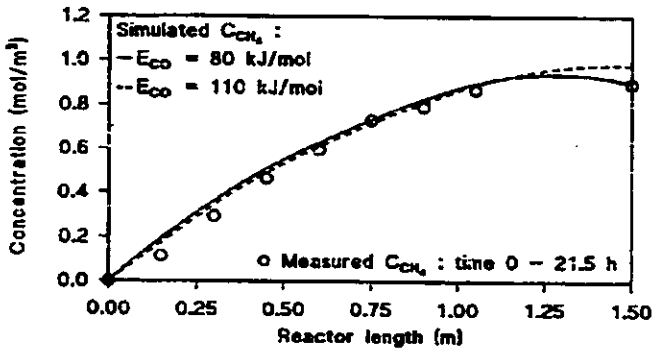

Wall heat conduction model. Wall function: Equation 5–13

Figure 5–11c. Comparison of simulated and measured CH_4 profiles. Run no 1.

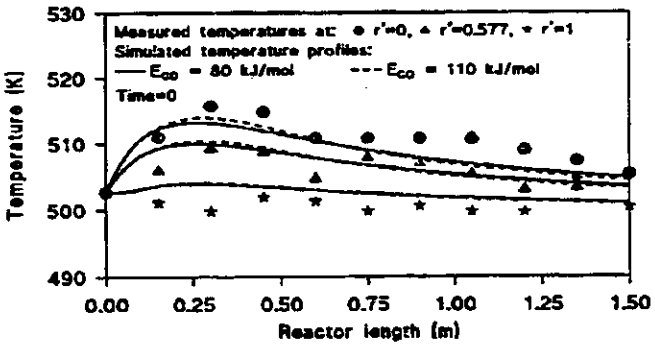

Wall heat transfer model.

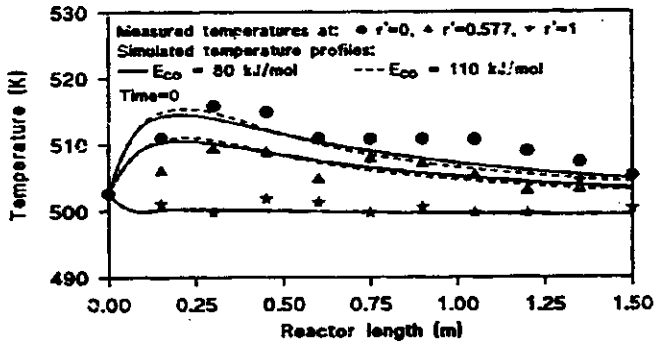

Wall heat conduction model.
Wall function:
Equation 5–12
L_w = 1.0

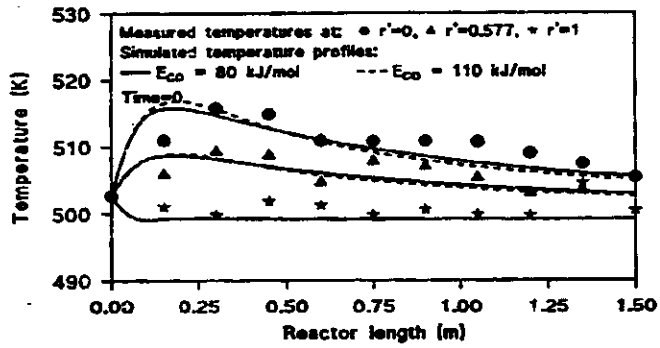

Wall heat conduction model.
Wall function:
Equation 5–13

Figure 5–12a. Comparison of simulated and measured temperature profiles. Run no 2.

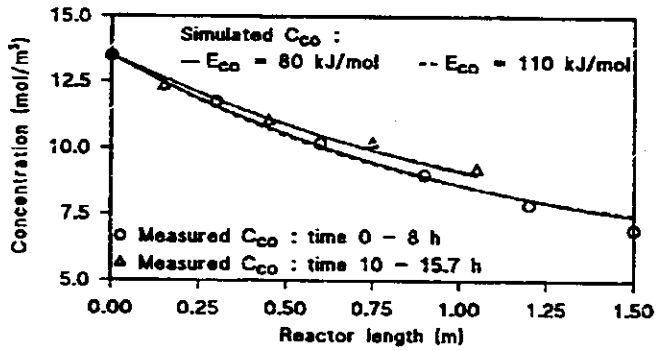

Wall heat transfer model.

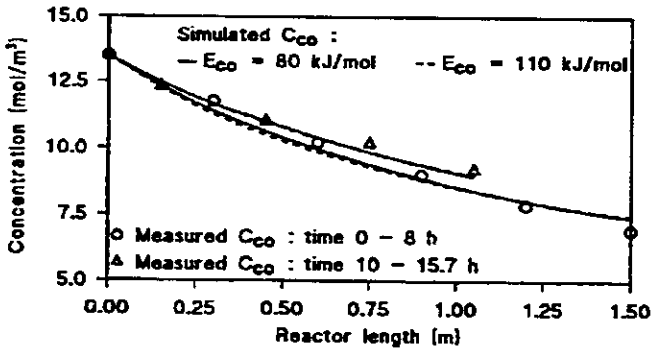

Wall heat conduction model. Wall function: Equation 5–12 $l_w = 1.0$

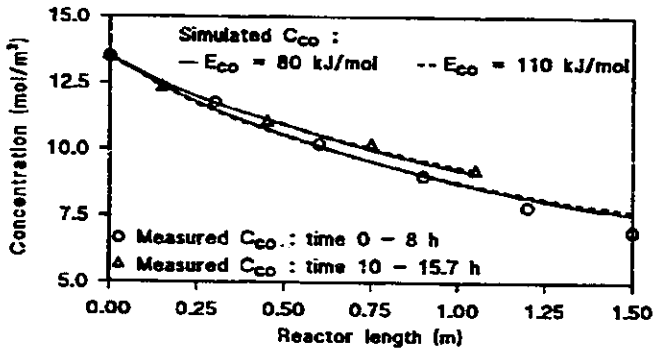

Wall heat conduction model. Wall function: Equation 5–13

Figure 5–12b. Comparison of simulated and measured CO profiles. Run no 2.

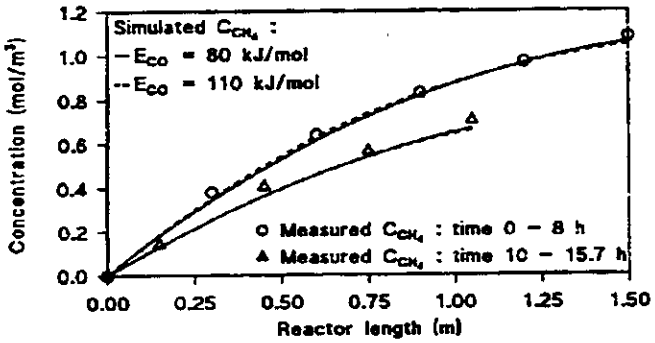

Wall heat transfer model.

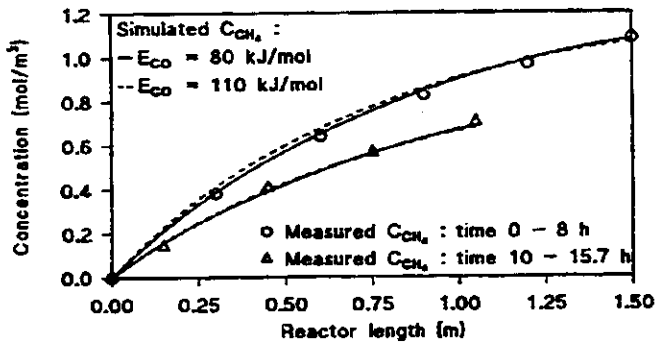

Wall heat conduction model.
Wall function:
Equation 5–12
l_w = 1.0

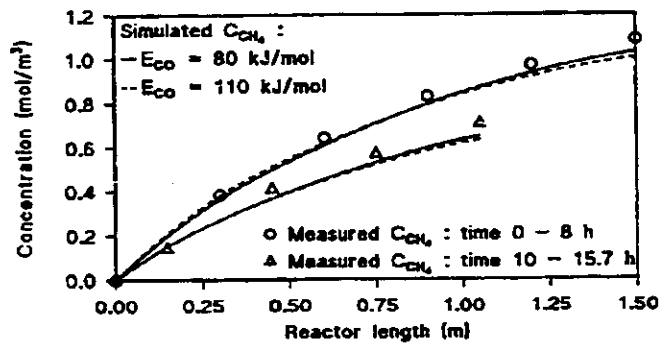

Wall heat conduction model.
Wall function:
Equation 5–13

Figure 5–12c. Comparison of simulated and measured CH_4 profiles. Run no 2.

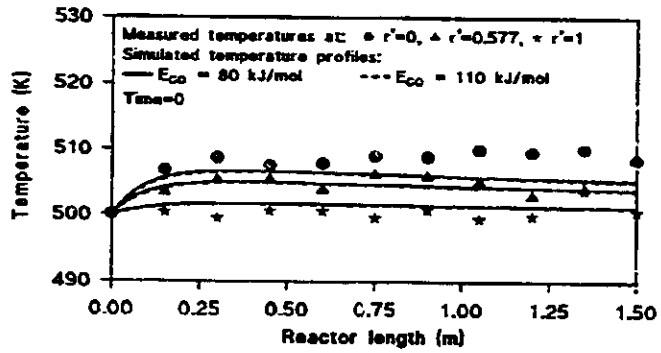

Wall heat transfer model.

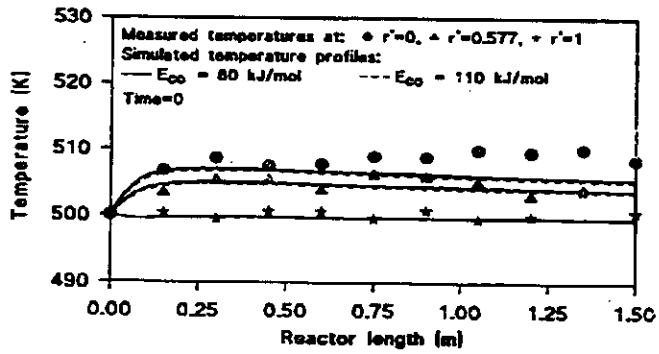

Wall heat conduction model.
Wall function:
Equation 5–12
l_w = 1.0

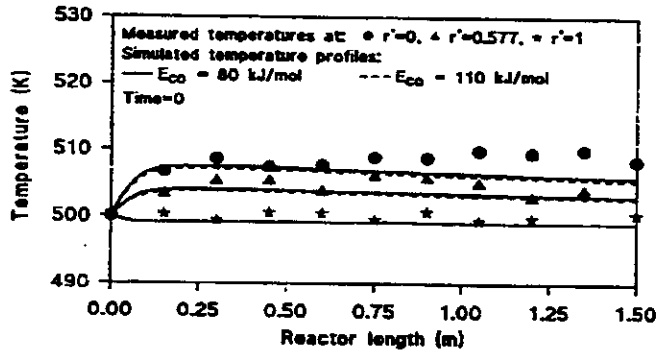

Wall heat conduction model.
Wall function:
Equation 5–13

Figure 5–13a. Comparison of simulated and measured temperature profiles. Run no 3.

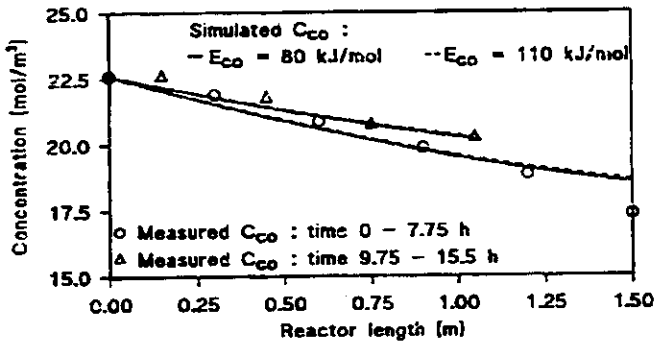

Wall heat transfer model.

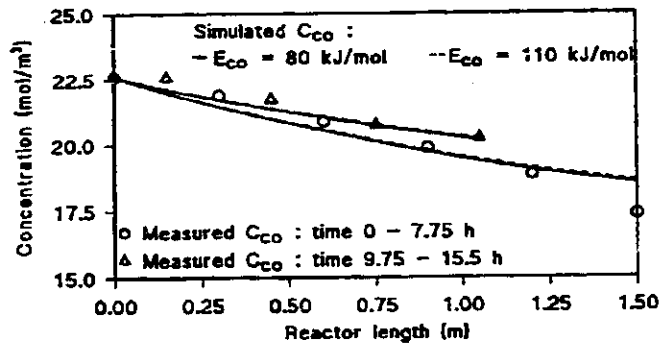

Wall heat conduction model. Wall function: Equation 5–12 l_w = 1.0

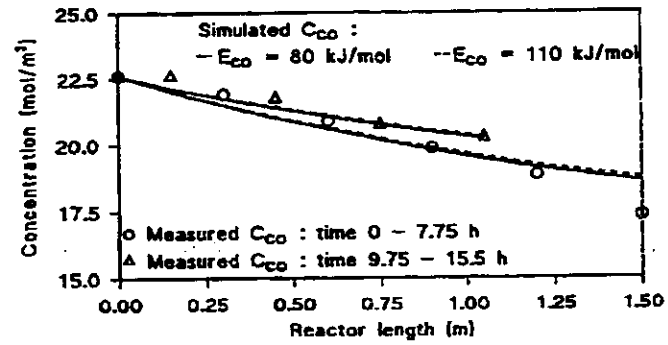

Wall heat conduction model. Wall function: Equation 5–13

Figure 5–13b. Comparison of simulated and measured CO profiles. Run no 3.

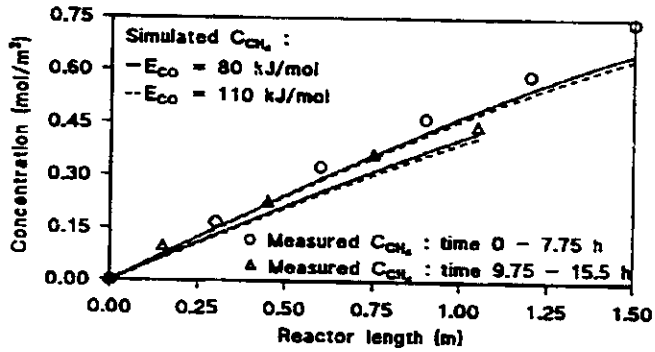

Wall heat transfer model.

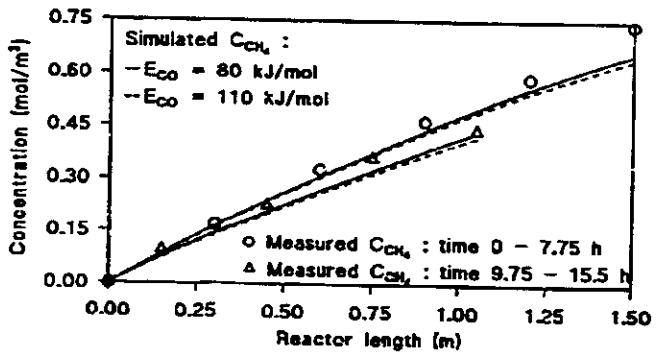

Wall heat conduction model. Wall function: Equation 5–12 L_w = 1.0

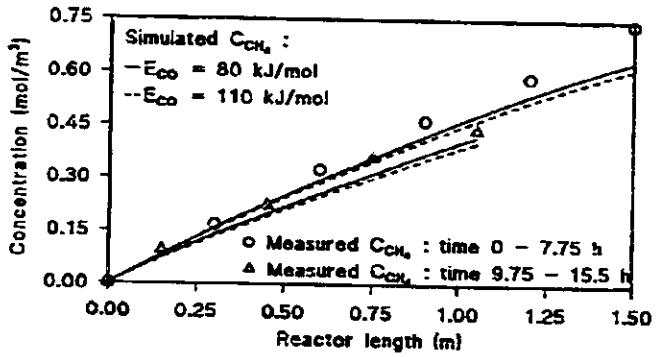

Wall heat conduction model. Wall function: Equation 5–13

Figure 5–13c. Comparison of simulated and measured CH_4 profiles. Run no 3.

Generally the differences between calculated concentration profiles are small when comparing between the different model assumptions. This is also the case when comparing concentration profiles from the plug flow model, using measured axial temperature profiles employed in estimation of the kinetic parameters, with the profiles from the models including heat transfer.

There is virtually no effect of the two assumptions made on the values of the activation energies on the calculated temperature and concentration profiles. Only a weak correlation was found between activation energy and the heat transfer parameters. For all the models the conductivity of the bed had to be increased for the highest activation energies compared with the lower, but the effect was generally less than 5% on estimated heat transfer parameters. This was not unexpected since the differences in temperature across the bed were small. In this case the interaction between kinetics and heat transfer becomes weak.

For the wall heat transfer model the estimated value of the fluid–mechanical Peclet number, Pe^{4}_{ar}, was about 6.9. This is considerably lower than the theoretical value of 11.7 calculated from equation 2–25 (Schlünder, 1966). Thus the apparent effective thermal conductivity of the bed estimated under reactive conditions was about 70% higher than the value predicted by equation 2–25. It is reported that calculated values from this relation compares well with experimental radial dispersion data from several investigations (Tsotsas and Schlünder, 1988), obtained by injection measurements under non–reactive conditions.

It is a common observation that effective radial conductivities estimated from measurements under reactive conditions are considerably higher than those obtained from cold–flow measurements using the wall heat transfer model, e.g. (Paterson and Carberry, 1983; Schwedock et al., 1989b; Daszkowski and Eigenberger, 1992). This overestimation of the effective conductivity leads to calculated temperature differences which are smaller than the measured ones as shown in Figures 5–11a, 5–12a and 5–13a.

Some of the simulation results from the wall heat conduction models with radial variations in void fraction, velocity and conductivity showed better adaption to the measured wall temperatures than simulations from the wall heat transfer model. But the simulated temperature profiles show a significant dependence on the assumptions made about the

variation in conductivity in the near–wall region. This dependence is also reflected in the estimated values of the constant C in equation 5–6.

Inclusion of the wall function equation 5–7 with l_w=1 gives C=0.24. This corresponds to a conductivity in the interior of the bed of about 0.75 W/m K which is comparable with the value estimated from the wall heat transfer model. As seen from Figures 5–11a, 5–12a and 5–13a the temperature differences in the interior of the bed are about the same for the two cases.

With l_w=2.5 the constant C was estimated to be about 0.5 which corresponds to a rather high interior conductivity. The temperature profiles for this case is not shown in the Figures, but internal temperature differences were much smaller than the measured ones. So this was clearly an unrealistic case.

Simulated temperature profiles for the case of no extra wall function in equation 5–6 are also shown in Figures 5–11a, 5–12a and 5–13a. This case seems to give the best fit between simulated and measured temperature profiles of the models considered in this study. The value obtained for C was about 0.10 which corresponds to an internal conductivity of about the half of the value obtained for the wall heat transfer model.

These results indicate that the wall heat conduction model with radial variations in void fraction, velocity and thermal conductivity is able to give a more realistic representation of a fixed bed reactor than the traditional dispersion models. But the wall heat conduction model is rather sensitive to assumptions made on the variations in conductivity in the near–wall region. Since the conductivity is dependent on local velocity, the radial velocity profile is an important factor in determining radial temperature profiles.

Comparison of calculated temperature profiles from the heat conduction model with the experimental temperature profiles shows that the calculated profiles are steeper near the inlet, reaching maximum before the measured profiles. This ambiguity is not readily explained, but generally the wall heat conduction model gives a more pronounced temperature profile with an earlier maximum than the wall heat transfer model. This is due to the channeling in the

near wall region and subsequent lower velocity in the core of the bed for the wall heat conduction model. In addition, when including the radial void fraction profile, the catalyst density in the core of the bed is higher than in the near–wall region giving higher reaction rates in the interior of the bed than predicted by the wall heat transfer model. Lower conductivity in the core region will also give more pronounced profiles with an earlier maximum.

An explanation of the observed discrepancy could be that the build–up of the radial velocity profile occurs over some distance from the inlet. This is, however, not a likely explanation from the results of Daszkowski and Eigenberger (Daszkowski and Eigenberger, 1992) who state that the build–up of the radial flow profile mainly takes place in the first particle layer.

There are some uncertainities in the underlying assumptions of the wall heat conduction models which must be considered. The model rely on the radial void fraction profile described by equation 2–28 and not on a measured profile from the packed bed used in this study. Equation 2–28 is based on a bed packed with spherical particles, and is only an approximation of the real profile. In addition, measured void fraction profiles are dependent on catalyst particle geometry as shown in Appendix IV. Equation 2–28 was, however, used in this study due to lack of data on void fraction profiles for cylindrical particles.

If the assumed void fraction profile is wrong, then the velocity profile calculated from the relation given in Appendix IV becomes wrong. This is also the case if the empirical factors used in the momentum balance equation 2–29 are wrong. Verification of calculated flow profiles by direct measurements in the bed is practically impossible without disturbing the flow pattern.

These uncertainities regarding void fraction and velocity profiles also make it impossible to give any clear statements as to the correctness of including a wall function in the expression used to calculate local conductivity, and eventually the nature of this function. This is due to the sensivity of calculated temperature profiles on the details of variations in thermal conductivity in the near-wall region and the uncertainities as to what is the real velocity profile in this region.

Finally the question of axially varying catalyst activity adds to these previous questions as discussed in chapter 5.3.3. Varying activity will clearly influence the measured profiles.